Charge-changing interactions of ultrarelativistic Pb nuclei

C. Scheidenberger,[1] I. A. Pshenichnov,[1,2,3] K. Sümmerer,[1] A. Ventura,[4,5] J. P. Bondorf,[2] A. S. Botvina,[1,3] I. N. Mishustin,[2,6,7] D. Boutin,[1] S. Datz,[8,*] H. Geissel,[1,9] P. Grafström,[10] H. Knudsen,[11] H. F. Krause,[8] B. Lommel,[1] S. P. Møller,[11] G. Münzenberg,[1] R. H. Schuch,[12] E. Uggerhøj,[11] U. Uggerhøj,[11] C. R. Vane,[8] Z. Z. Vilakazi,[13] and H. Weick[1]

[1]*GSI, Planckstraße 1, D-64291 Darmstadt, Germany*

[2]*Niels Bohr Institute, DK-2100 Copenhagen, Denmark*

[3]*Institute for Nuclear Research, Russian Academy of Science, 117312 Moscow, Russia*

[4]*Italian National Agency for New Technologies, Energy, and the Environment, I-40129 Bologna, Italy*

[5]*National Institute for Nuclear Physics, Bologna Section, Italy*

[6]*Institut für Theoretische Physik, J.W. Goethe Universität, D-60054 Frankfurt am Main, Germany*

[7]*Kurchatov Institute, Russian Research Center, 123182 Moscow, Russia*

[8]*Oak Ridge National Laboratory, Oak Ridge, Tennessee 38731, USA*

[9]*II. Physikalisches Institut, Justus-Liebig-Universität Gießen, Heinrich-Buff-Ring 14-16, D-35392 Gießen, Germany*

[10]*CERN, CH-1211 Geneva, Switzerland*

[11]*Institute for Physics and Astronomy, Aarhus University, DK-8000 Aarhus C, Denmark*

[12]*Atomic Physics Department, Stockholm University, Frescativägen 24, S-10405 Stockholm 50, Sweden*

[13]*Department of Physics, University of Witwatersrand, 1 Jan Smuts Avenue, P O Wits, Johannesburg 2050, South Africa*

(Received 5 November 2003; published 29 July 2004)

Experimental data and theoretical results on charge loss $-27 \leqslant \Delta Z \leqslant -1$, charge pickup $\Delta Z = +1$, and total charge-changing cross sections for 158*A* GeV $^{208}_{82}$Pb ions on CH_2, C, Al, Cu, Sn, and Au targets are presented. Calculations based on the revisited abrasion-ablation model for hadronic interaction and the relativistic electromagnetic dissociation (RELDIS) model for electromagnetic interaction describe the data. The decay of excited nuclear systems created in both types of interaction is described by the statistical multifragmentation model (SMM), which includes evaporation, fission, and multifragmentation channels. We show that at very high projectile energy the excitation energy of residual nuclei may be described on average as ~40 MeV per removed nucleon, with some increase in this value compared to fragmentation of intermediate energy heavy ions at ~1*A* GeV. The importance of the electromagnetic interaction in production of $_{80}$Hg, $_{81}$Tl, and $_{83}$Bi projectile fragments on heavy targets is shown. A strong increase of nuclear-charge pickup cross sections, forming $_{83}$Bi, is observed in comparison to similar measurements at 10.6*A* GeV. This process is attributed to the electromagnetic production of a negative pion by an equivalent photon, which is quantitatively described by the RELDIS model.

DOI: 10.1103/PhysRevC.70.014902 PACS number(s): 25.75.−q, 24.10.Jv

I. INTRODUCTION

Measuring nuclear charge-changing cross sections is a simple and explorative way to establish the global features of high-energy nuclear reactions for those cases where little is known experimentally. Inclusive cross sections for producing a fragment of charge Z from a projectile nucleus of charge Z_1 are measured with results presented as a function of $\Delta Z = Z - Z_1$. As an example, the gross features of ^{238}U fragmentation at 900*A* MeV can be established by simply measuring the energy-deposition of the fragments in a stack of Si detectors [1]. Such measurements also supply data relevant to other fields of research, e.g., cosmic ray propagation and nuclear astrophysics [2].

By varying the atomic number of the reaction targets, the contributions from hadronic and electromagnetic interactions can be disentangled. In a similar way, survey measurements of the fragmentation of ultrarelativistic ^{208}Pb nuclei have been performed in terms of charge-changing processes [3–6]. These results allowed us, e.g., to identify the relevance of electromagnetic processes in charge-pickup reactions [5], where the nuclear charge Z_1 of the projectile is *increased*, $\Delta Z = +1$. As shown by calculations based on the relativistic electromagnetic dissociation (RELDIS) model [7], the electromagnetic interaction with π^- production by virtual photons is responsible for a dominant part of charge-pickup reactions at ultrarelativistic energies on medium-weight and heavy targets [5].

The present study complements an earlier analysis [5] that was focused on the nuclear-charge pickup ($\Delta Z = +1$). In this paper, we present new data on nuclear-charge-loss cross sections ($\Delta Z < 0$), which are mainly determined by hadronic interactions. Since we use electronic detectors instead of nuclear track detectors, the statistical significance of our data is expected to be larger than that of Refs. [3,4,6]. On the other hand, our ionization chamber resolves individual nuclear-charge peaks only down to $Z = 55-60$, whereas the track-detector experiment [3,6] was able to cover a much wider range of fragment charges ($7 \leqslant Z \leqslant 81$). Thus the two experimental approaches can be considered complementary to each other.

*Deceased.

The present data together with the data of Refs. [3,6] open a new opportunity to gain more insight into the underlying physical processes than a mere parametric fit of the cross sections. Below we will present a theoretical interpretation of these data on the basis of two well established models, the abrasion-ablation model for hadronic interactions and the RELDIS model for electromagnetic interactions of relativistic heavy ions. The following questions are addressed in our theoretical analysis: (1) How can one estimate the excitation energy of a nuclear system formed by sudden removal of several nucleons? (See Sec. III A 2). (2) Since several estimates for the excitation energy are known from the literature, how are they related to each other and how successful are they in describing data well above 1*A* GeV? (See Secs. III A and IV B). (3) To which extent does electromagnetic interaction contribute to charge-changing reactions and how does this contribution depend on projectile energy and target mass? (See Sec. IV C).

In Sec. II, we first present the experimental setup, the data analysis procedure, and the measured results. Section III is devoted to the description of theoretical approaches. First, we discuss the abrasion-ablation model, with the main emphasis on the question how to calculate the excitation energies of a prefragment after the abrasion stage. Then we give a short review of the RELDIS model for calculating electromagnetic processes at relativistic energies. In Sec. IV we compare our data to the model calculations. Our conclusions are presented in Sec. V.

II. EXPERIMENT

The present experiment is primarily aimed at the study of nuclear-charge-changing cross sections of 158*A* GeV ^{208}Pb projectiles on various target materials ranging from hydrogen to gold. The key feature of the present experiment is the use of an ionization chamber as the *Z*-sensitive detector. Compared to nuclear-track detectors [3,6], the small areal density of the ionization chamber induces much less secondary reactions. In addition, much better statistics is obtained than in the track-detector experiment [3,6].

A. Experimental setup

The experiment was carried out at the H2-beamline in the North Hall of the CERN Super Proton Synchrotron (SPS) accelerator facilities. The experimental setup consisted of a scintillator detector and two charge-sensitive multiple sampling ionization chambers (MUSICs) [8], between which the reaction targets were mounted (see Fig. 1). With the first MUSIC (MUSIC1, in front of the targets) the incoming Pb ions were counted, whereas the second MUSIC (MUSIC2, behind the targets) registered the atomic numbers of the outgoing reaction products. The entire setup was about 2 m long and was placed in air between two vacuum windows of the beam pipe.

The scintillator detector consisted of 100 μm thick BC418 material with a diameter of 20 mm and delivered a fast trigger signal for each incoming ion. The MUSICs had active volumes of 36 cm length (in the beam direction) and

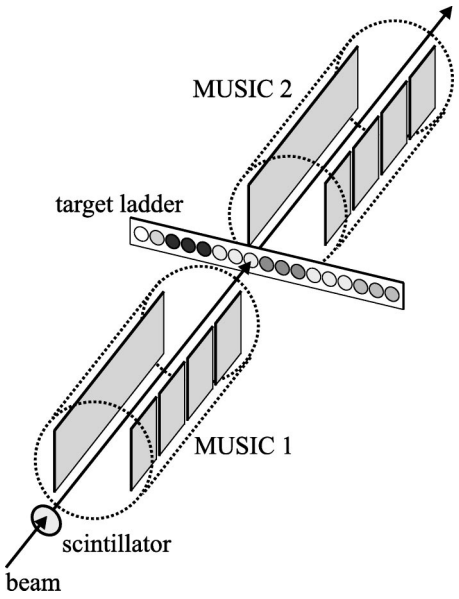

FIG. 1. Schematic view of the experimental setup. The reaction targets are placed between two multiple-sampling ionization chambers (MUSIC) with fourfold segmented anodes. A trigger signal of the incoming beam is obtained from the scintillator detector.

areas of 20×20 cm^2 (perpendicular to the beam axis). They were operated with P10 gas (90% argon, 10% methane) at normal temperature and pressure and had fourfold segmented anodes. Each ion penetrating through the detector deposits energy and thus creates electron-ion pairs, the number of which is to first order proportional to the square of the projectile charge. The free electrons are collected at the anodes, charge-sensitive preamplifiers transform the charge to proportional voltages, which are amplified and shaped with a shaping-time constant of 1 μs and finally digitized with a CAMAC analog-to-digital converter (ADC). The readout was triggered by the scintillator signal and the data were recorded event by event with the data acquisition system CAMDA [9]. The timing outputs were used to determine the horizontal positions of the ions. The time between the scintillator signal and the arrival of the electrons at the anode is governed by the drift time of the electrons, which is directly related to the projectile position by means of the drift velocity of about 5 cm/μs under the applied operating conditions. In the off-line analysis this position information was used to suppress scattered ions (approximately 1%), which did not hit the targets. The four energy signals of each MUSIC were averaged and yielded the nuclear-charge spectra, from which the charge-changing cross sections were derived. The charge resolution (standard deviation) amounts to 0.3 charge units. Spectra obtained with different targets are shown in Fig. 2.

The targets had diameters of 45 mm and were mounted on a remotely controlled, horizontally movable ladder placed between the two MUSICs. One polyethylene (CH_2) target and three targets of each of the following elements were used: carbon, aluminum, copper, tin, and gold. Their thicknesses covered areal weights ranging from 0.31 g/cm^2 to 6 g/cm^2 corresponding to total nuclear-interaction probabilities ranging from approximately 5% to 20%.

The beam was extracted at a kinetic energy of 158*A* GeV, had a spill length of 5 s, a horizontal width of 3 mm (stan-

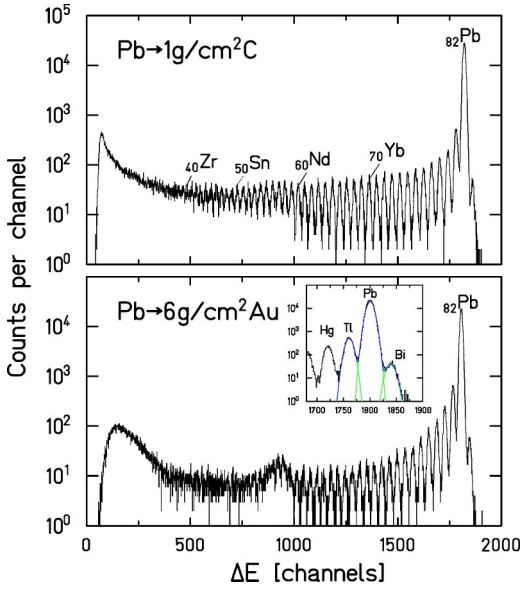

FIG. 2. (Color online) Energy-deposition spectra obtained with MUSIC 2 for an incoming 158*A* GeV Pb ion beam and two different targets (upper spectrum: 1 g/cm^2 carbon target, lower spectrum: 6 g/cm^2 gold target). The inset in the lower spectrum shows an enlarged part of the spectrum with the heaviest reaction products. The bismuth peak, which arises from nuclear-charge pickup ($\Delta Z=+1$) is clearly visible.

dard deviation), and an angular divergence of 50 μrad (standard deviation). The intensity of the incident beam was varied during the measurements between 300 ions per second and 10^4 ions per second depending on the needs of another experiment running simultaneously at the same beamline [10]. The first MUSIC was used to identify the incoming Pb ions, i.e., to exclude those ions from the analysis that had undergone nuclear-charge changing reactions in vacuum windows and detectors upstream in the beamline, which could not be removed during the measurements.

B. Data analysis and numerical results

For each individual target, the total charge-changing cross section σ_{cc} is obtained from the measured survival probability $\mathcal{R}_1$, the empty-target correction $\mathcal{R}_0$, and the target thickness *nd* by the equation

$$\sigma_{cc} = \ln(\mathcal{R}_0/\mathcal{R}_1)/nd. \quad (1)$$

The target thickness *nd* is the number of target atoms per unit area in the case of monatomic materials and the number of CH_2 molecules in the case of the polyethylene target. The ratio $\mathcal{R}_1 = N_1'(Z=82)/N_1(Z=82)$ is determined from the number of noninteracting Pb ions, $N_1'(Z=82)$, counted in the second MUSIC behind the target, and $N_1(Z=82)$ is the number of incoming Pb ions counted with the first MUSIC in front of the target, and $\mathcal{R}_0$ is the analogous quantity determined in a targetless exposure in order to determine the number of reactions in material other than the interaction target, e.g., in the MUSIC detectors and in air. This latter total charge-changing reaction probability without target, $\mathcal{R}_0$, amounts to $(1.5\pm0.1)\%$ and leads to a small correction only.

For the measurements with each individual target, between 3×10^5 and 1.1×10^6 incoming Pb ions were recorded. The cross section errors are estimated from the uncertainty of the target-thickness determination (which is accurate to better than 1%) and from the statistical contribution in the determination of the numbers $N_i(Z=82)$ and $N_i'(Z=82)$, with $i=0,1$. For all target materials investigated, the cross sections determined for the different thicknesses agree with each other within the experimental errors (i.e., no systematic thickness dependence is observed) and are therefore averaged to obtain the final values. The cross sections for hydrogen are calculated from the measured cross sections for polyethylene and carbon according to $\sigma_H = 0.5(\sigma_{CH_2} - \sigma_C)$, where σ_{CH_2} is the cross section per CH_2 molecule.

Partial charge-changing cross sections $\sigma(Z)$ have been obtained in a similar way from the measured charge spectra as shown in Fig. 2 by determining the number of created ions $N_i'(Z)$, where Z denotes the atomic number of the outgoing fragment after charge loss $\Delta Z = Z - 82$. The special case of charge pickup, where Bi ions are produced with $Z=83$ and thus $\Delta Z=+1$, has been described in Ref. [5]. For these reactions, the partial charge-changing probability is much smaller than unity in the targets used, and thus the logarithm in Eq. (1) can be expanded and the cross sections is simply determined from $\sigma(Z) = [\mathcal{R}_1(Z) - \mathcal{R}_0(Z)]/nd$, where $\mathcal{R}_i(Z) = N_i'(Z)/N_i(Z=82)$. In particular, the single-collision condition is fulfilled and two- and more-step reactions can safely be ignored.

All experimental values for partial and total charge-changing cross sections obtained from the present analysis are given in Tables I and II, respectively, and are visualized in Figs. 3 and 4, respectively. As shown in Fig. 3, our data for charge loss have the same general trend as recent data [6] obtained with CR39 nuclear track detectors. The data of Ref. [6] have larger statistical ($\sim$10%) and systematic ($\sim$8%) uncertainties compared to our data. The difference between the data sets far exceeds these values for some individual cross sections, but the only systematic deviation between the sets of data is found for Al targets. Less agreement is found for data on hydrogen target, where the data of Ref. [6] have larger overall uncertainty ($\sim$25%). Concerning charge-pickup data obtained in both experiments, good agreement is found for C targets, and less satisfactory for Al and Cu. The heaviest target nucleus in Ref. [6] is Pb, to be compared to Au in our experiment, and our charge-pickup cross section is approximately three times the value of Ref. [6]. However, this difference may be caused by a large statistical error for the value of Ref. [6].

Finally, our measured total charge-changing cross sections are given in Table II and shown in Fig. 4 combined with data of Ref. [6]. The results of both experiments are in very good agreement for this integral characteristic of fragmentation reaction and can be described well by theory, as will be elaborated in the following sections. Here we mention only that the value for the Cu target of Ref. [6] is somehow below both our experimental result and theoretical prediction.

III. THEORY

Below, A_1 and Z_1 (A_2 and Z_2) denote mass number and charge of the projectile (target) nucleus, respectively. One

TABLE I. Measured partial charge-changing cross sections $\sigma(Z)$ in millibarn for 158*A* GeV ^{208}Pb ions on H, C, Al, Cu, Sn, and Au targets.

Z	H	C	Al	Cu	Sn	Au
83	$5.4^{+1.9}_{-3.6}$	9.4±2.8	15.4±2.3	37.4±5.4	73.2±6.4	148.2±15.2
81	147.7±4.5	193.0±3.2	246.2±6.5	548.4±12.5	974.1±13.4	2227.0±36.9
80	79.4±2.7	102.6±2.0	129.2±4.3	234.2±6.8	428.0±8.2	955.0±23.8
79	57.9±2.3	71.7±1.7	78.3±3.3	151.6±5.7	261.2±6.6	526.2±17.8
78	47.4±2.2	56.5±1.6	59.8±3.1	104.6±5.3	144.3±5.2	313.3±14.8
77	39.4±2.0	49.9±1.5	49.2±2.7	85.8±4.5	107.4±4.4	220.3±18.0
76	35.1±2.0	41.2±1.4	43.2±2.7	63.1±4.4	87.7±4.5	141.3±20.9
75	28.9±0.2	38.7±0.2	36.6±0.3	57.6±0.5	72.8±0.5	130.2±10.1
74	32.2±0.2	33.6±0.2	37.7±0.4	47.3±0.4	72.7±0.9	99.2±4.6
73	30.9±0.2	31.9±0.1	32.3±0.4	49.8±0.5	59.5±1.1	86.8±5.6
72	28.6±0.2	32.6±0.1	31.7±0.3	40.9±0.4	52.9±1.1	85.4±11.7
71	26.6±0.2	28.5±0.2	33.0±0.4	40.1±0.4	50.0±0.9	67.4±11.2
70	26.7±0.2	28.7±0.2	27.8±0.4	41.7±0.4	45.9±0.9	78.5±11.1
69	27.4±0.1	25.3±0.1	29.8±0.4	34.1±0.4	44.4±1.2	54.3±10.1
68	24.7±0.1	24.8±0.1	25.1±0.4	31.3±0.4	45.7±1.2	68.2±10.5
67	22.9±0.1	25.6±0.1	28.8±0.4	32.9±0.4	35.3±4.3	43.6±10.5
66	22.7±0.1	24.2±0.1	26.7±0.4	34.3±0.5	43.3±18.	59.0±9.5
65	23.3±0.1	22.8±0.2	27.1±0.4	34.3±0.4	34.1±0.3	46.3±9.6
64	21.6±0.1	23.3±0.1	22.9±0.3	28.4±0.4	32.9±0.3	47.8±9.7
63	21.0±0.2	22.6±0.2	24.8±0.4	31.8±0.4	40.1±0.3	45.1±8.9
62	20.1±0.1	23.3±0.1	27.8±0.5	26.8±0.5	31.3±0.3	45.1±11.3
61	20.2±0.1	20.7±0.2	19.5±1.3	30.9±0.6	32.1±0.3	39.8±12.6
60	19.5±0.2	22.1±0.2	23.7±1.9	32.7±0.5		38.3±10.8
59	20.5±0.2	23.1±0.2	21.4±2.1			
58	26.1±0.1	24.1±0.1	29.1±1.1			
57	31.1±0.3	26.0±0.3	21.9±0.9			
56	27.0±0.3	30.8±0.3	35.9±0.7			
55	24.5±0.2	20.9±0.1				

can expect that two types of interactions change the nuclear charge of the projectile. In hadronic collisions with impact parameter $b \leqslant R_1 + R_2$, where R_1 and R_2 are the nuclear radii, direct proton removal from the projectile and charge-changing elementary nucleon-nucleon (NN) interactions between collision partners are possible. Projectile charge loss is also possible in electromagnetic interactions between the colliding nuclei via their excitation and subsequent decay, or direct spallation of nuclei by virtual photons. These processes dominate at impact parameters $b \geqslant R_1 + R_2$. They are especially important for heavy targets at ultrarelativistic energies. As demonstrated in Fig. 4, electromagnetic processes contribute up to ~50% to the total charge-changing cross section in PbAu and PbPb collisions.

Below we assume that the domains of nuclear and electromagnetic interactions are separated by an impact parameter b_c, which is chosen according to the Benesh-Cook-Vary (BCV) parametrization of Ref. [11]:

$$b_c = R_{BCV}[A_1^{1/3} + A_2^{1/3} - X_{BCV}(A_1^{-1/3} + A_2^{-1/3})]. \qquad (2)$$

The values $R_{BCV} = 1.34$ fm and $X_{BCV} = 0.75$ were found from a fit to Glauber-type calculations of the total nuclear reaction cross sections, (Ref. [11]). Approaches for calculating these two contributions to charge-changing reactions are considered in Secs. III A and III B.

TABLE II. Measured total charge-changing cross sections σ_{cc} in barns for 158*A* GeV ^{208}Pb ions on H, C, Al, Cu, Sn, and Au targets.

H	C	Al	Cu	Sn	Au
1.57±0.06	3.00±0.06	3.75±0.08	5.51±0.17	7.67±0.15	11.40±0.34

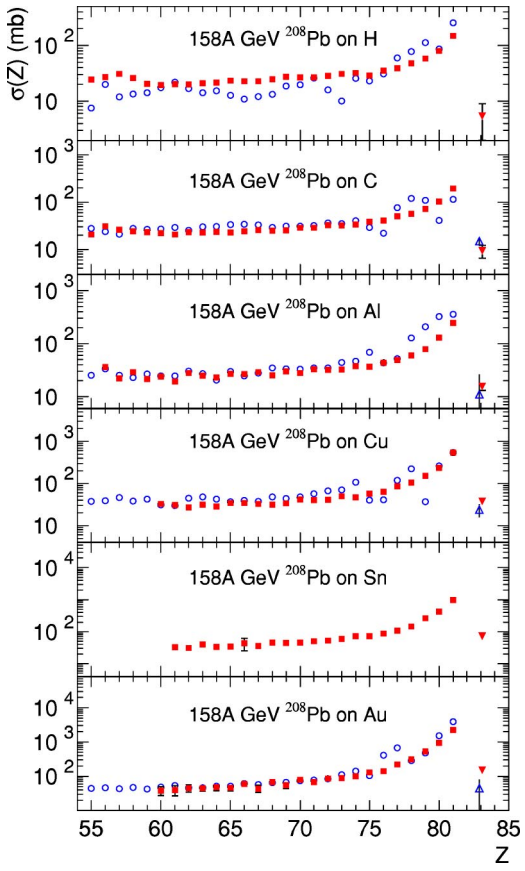

FIG. 3. (Color online) Measured partial charge-changing cross sections for charge-loss ($\Delta Z<0$, full squares) and charge-pickup ($\Delta Z=+1$, full triangles) cross sections of 158*A* GeV ^{208}Pb ions on H, C, Al, Cu, Sn, and Au targets from the present work. For comparison, the data of Ref. [6] for charge-loss and charge-pickup cross sections are shown by the open circles and triangles, respectively. The data on PbPb interactions [6] are presented in the bottom panel to be compared with our PbAu measurements Error bars are plotted in the figure, but are in most cases smaller than the size of the symbols and may thus be not visible.

A. Fragmentation in hadronic interactions

Hadronic interactions of ions take place in the range of impact parameters b from complete overlap of nuclei in central collisions, $b\simeq 0$, up to grazing interactions in peripheral collisions, $b\simeq R_1+R_2$. Such violent nuclear collisions at intermediate energies $\sim 1A$ GeV are commonly described within the framework of a participant-spectator (abrasion-ablation) model [12–14], where participants originate from the overlapping parts of the colliding nuclei, while their non-overlapping parts are treated as spectators. At relativistic energies nucleons from the participant zone are kinematically well separated (abraded) from spectators, which represent excited remnants of the initial nuclei (prefragments).

Finally, nuclear fragments are formed after secondary decays of these prefragments in a so-called ablation process originally described by statistical evaporation and fission models [12–14]. As shown below, this picture remains valid also for fragment production at ultrarelativistic energies, $\sim 10-100$ *A* GeV, and a common set of parameters describing the correlation between the prefragment mass and excitation energy may be used in both energy domains. However, we use the statistical multifragmentation model (SMM) [15–18] to describe realistically the breakup of highly excited nuclear systems in the ablation step.

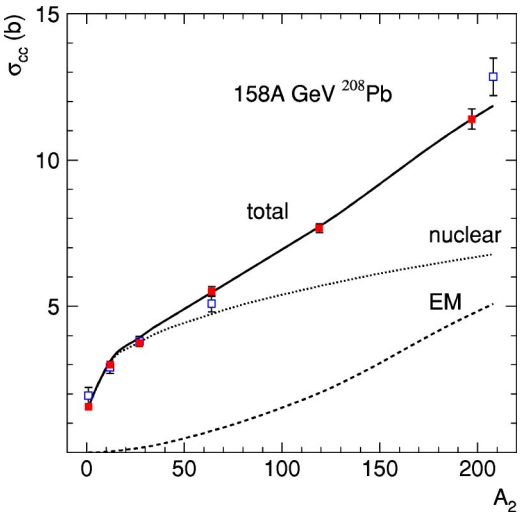

FIG. 4. (Color online) Total charge-changing cross sections of the present work (full squares) for 158*A* GeV Pb ions as a function of target mass number A_2. The data of Ref. [6] are shown by the open squares. Electromagnetic contribution calculated by the RELDIS code and nuclear contribution calculated within the abrasion-ablation model are shown by the dashed and dotted lines, respectively. The solid curve is the sum of both contributions.

1. Abrasion step

The cross section for the abrasion of a nucleons from the projectile (A_1,Z_1) in a collision with the target (A_2,Z_2) may be derived from the Glauber semiclassical theory of multiple scattering [12]:

$$\sigma^{abr}(a)=\binom{A_1}{a}2\pi\int_0^{b_c} b\,db[1-P(b)]^a P(b)^{A_1-a}. \qquad (3)$$

Here $P(\vec{b})$ is calculated as the overlap of projectile, $\rho_1(\vec{r})$, and target, $\rho_2(\vec{r})$, densities in a collision with impact parameter b:

$$P(\vec{b})=\int d^2\vec{s}D_1(\vec{s})\exp[-A_2\sigma_{NN}D_2(\vec{s}+\vec{b})], \qquad (4)$$

where the nuclear thickness functions,

$$D_{1,2}(\vec{s})=\int_{-\infty}^{+\infty} dz\ \rho_{1,2}(\vec{s},z), \qquad (5)$$

are introduced. The nuclear density profiles are approximated by the Fermi functions:

$$\rho_{1,2}(r) = \frac{\rho_0}{1 + \exp\left(\frac{r - r_0 A_{1,2}^{1/3}}{d}\right)}, \tag{6}$$

where $R_{1,2} = r_0 A_{1,2}^{1/3}$ is the nuclear half-density radius with $r_0 = 1.14$ fm being an average value between the proton and neutron distributions; $d = 0.54$ fm is the diffuseness parameter. For the total NN cross section a value of $\sigma_{NN} = 40$ mb was used in the calculations.

We use the same set of parameters for the abrasion process as in Ref. [7]. Data on dissociation of ^{197}Au nuclei into ^{196}Au$+n$ and ^{195}Au$+2n$ induced by 158A GeV Pb beams [22] were successfully described in Ref. [7] taking into account the abrasion step only. In collisions leading to $1n$ and $2n$ removal in the abrasion step, the excitation energy of prefragments is rather low so that subsequent nucleon emission is largely suppressed in the ablation step.

Only the total number of nucleons removed from the projectile is given by the above expressions. Further assumptions are needed to determine the numbers of protons, z, and neutrons, n, abraded from the initial nucleus. Corresponding distributions can be calculated by using the so-called hypergeometrical model [13,14], assuming there is no correlation between the proton and neutron distributions and the abrasion process removes protons and neutrons from the projectile nucleus in a random way:

$$\sigma^{abr}(n,z) = \frac{\binom{Z_1}{z}\binom{N_1}{n}}{\binom{A_1}{a}} \sigma^{abr}(a). \tag{7}$$

2. Estimation of prefragment excitation energy

An excited residual nucleus (prefragment) with mass $A_{pf} = A_1 - n - z$, charge $Z_{pf} = Z_1 - z$, and excitation energy E is created due to abrasion of a nucleons, $a = n + z$, from the projectile (A_1, Z_1). The corresponding differential cross section is given by

$$\frac{d\sigma^{abr}(A_{pf}, Z_{pf}, E)}{dE} = \sigma^{abr}(A_{pf}, Z_{pf}) w_a(E), \tag{8}$$

where $\sigma^{abr}(A_{pf}, Z_{pf}) = \sigma^{abr}(n,z)$ is defined by Eq. (7), and the probability distribution $w_a(E)$ to obtain the excitation energy E by removal of a nucleons is normalized according to $\int dE w_a(E) = 1$. The sum over different A_{pf}, Z_{pf} is equal to the total reaction cross section:

$$\sum_{A_{pf}, Z_{pf}} \sigma^{abr}(A_{pf}, Z_{pf}) = \sigma_R. \tag{9}$$

The inclusive cross section to produce a final fragment (A,Z) is then

$$\sigma(A,Z) = \sum_{A_{pf}, Z_{pf}} \sum_i \int dE \quad n_i(A,Z,E) \times f_i(E, A_{pf}, Z_{pf} \to A, Z) \sigma^{abr}(A_{pf}, Z_{pf}) w_a(E), \tag{10}$$

where f_i and n_i are, respectively, the branching ratio and number of fragments (A,Z) created by the decay of the prefragment (A_{pf}, Z_{pf}) with excitation energy E via a decay channel i.

The distribution $w_a(E)$ is a key input to the ablation step, where final fragments are produced by deexcitation of prefragments. We assume that evaluating the distribution of the excitation energy of a prefragment obtained by removing z protons and n neutrons from the primary nucleus amounts to computing the density of states of the nucleus with z proton holes and n neutron holes. For the sake of simplicity, we shall work out our formalism for only one type of nucleons.

Let $g(y)dy$ be the probability that one hole has an energy between y and $y+dy$, with $g(y)$ the density of one-hole states; thus, the density of a-hole states at excitation energy E is simply

$$\rho_a(E) = \frac{1}{a!} \int_0^\infty dy_1 \cdots dy_a g(y_1) \cdots g(y_a) \times \delta\left(E - \sum_{j=1}^{a} y_j\right). \tag{11}$$

In order to obtain the probability distribution $w_a(E)$ used in Eqs. (8) and (10), one has to divide $\rho_a(E)$ by the normalization integral: $w_a(E) = \rho_a(E) / \int dE' \rho_a(E')$. In the case when $g(y)$ is approximated by a simple analytic function, the integral in Eq. (11) can be given by a closed analytic expression. Here, following Gaimard and Schmidt [14], we assume that $g(y)$ is a linear function of y:

$$g(y) = g_0 - g_1 y \tag{12}$$

for $0 \leqslant y \leqslant E_{max}$, $g_0 > 0$ and $g_1 \geqslant 0$. When both g_0 and g_1 are different from zero, Eq. (12) is an approximation to the density of single-hole states in a spherical Woods-Saxon potential with a depth of the order of E_{max} [23]. The integral in Eq. (11) is calculated analytically with the result

$$\rho_a(E) = \sum_{m=0}^{a} \frac{(-1)^m}{m!\,(a-m)!\,(a+m-1)!} g_1^m g_0^{a-m} E^{a+m-1}. \tag{13}$$

The prefragment excitation-energy distributions, Eq. (13), for specific numbers of removed nucleons a are shown in Fig. 5 for $E_{max} = 40$ MeV.

When $g_1 = 0$, one gets the elementary equispaced model as a particular case. In this case only the $m = 0$ term survives, yielding a well-known Ericson formula [24] for the density of a-hole states:

$$\rho_{a_{Ericson}}(E) = \frac{g_0^a}{a!\,(a-1)!} E^{a-1}. \tag{14}$$

Some examples of prefragment excitation-energy distributions given by the Ericson formula are shown in Fig. 5 for

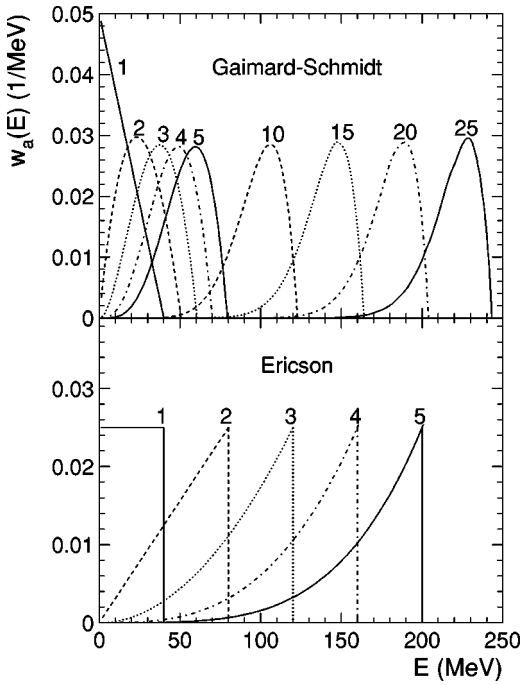

FIG. 5. Prefragment excitation-energy distributions created after the abrasion of a given number of nucleons. Top panel: distribution given by the Gaimard-Schmidt formula, Eq. (13), with $g_0 = 16\ \mathrm{MeV}^{-1}$, $g_1 = 0.4\ \mathrm{MeV}^{-2}$ for $a = 1-5, 10, 15, 20$, and 25. Bottom panel: distribution given by the Ericson formula ($g_1 = 0$) with $E_{max} = 40$ MeV for $a = 1-5$.

$E_{max} = 40$ MeV. The mean energy per removed nucleon is $\langle E \rangle = [a/(a+1)]E_{max}$. This gives $\langle E \rangle = 20$ MeV for the first nucleon removed, and $\langle E \rangle \sim 40$ MeV per removed nucleon for large a. The Ericson formula is widely used in preequilibrium models of low-energy nuclear reactions. On the other hand, the more general formula (13) leads to lower excitation energies per removed nucleon. For example, $\langle E \rangle = 13.3$ MeV for $a = 1$, $\langle E \rangle = 10.8$ MeV for $a = 5$, and $\langle E \rangle = 8.8$ MeV for $a = 25$. As shown in Fig. 5, the shapes of $\rho_a(E)$ are very different for the two cases Eqs. (13) and (14), which should be considered as two extreme approximations for prefragment excitation energy. It is worthwhile to stress that an even more general formula for the density of one-hole states, quadratic in the energy variable y, is worked out with the same method in Ref. [25], thus giving the Ericson and Gaimard-Schmidt formulas as particular cases.

A composite formula that corrects Eq. (14) for several effects, such as finite potential depth, Pauli principle, pairing effects, and the energy dependence of single-particle level densities, was recommended by the authors of Refs. [25,26]. For the sake of simplicity the proposed improvements are not used in the present paper. A reason for this simplification is that the approximation itself, which calculates the prefragment excitation energy E as the sum of the energies of holes left by abraded nucleons, contains uncertainties that exceed by far the differences due to the use of the composite formulas [25,26] instead of Eq. (14).

Indeed, several physical processes affecting prefragment excitation energies were neglected in the present approach. First, knocked-out nucleons can suffer a final state interaction with prefragments leading to excitation of nucleons to higher states and creation of additional holes. Second, hadrons produced in *NN* collisions may undergo subsequent interactions with prefragments and thus change their excitation energy. As known from other experiments performed at 158*A* GeV, the average value of 5 ± 0.2 pions per participating nucleon [27] may be given as an example. Third, the very structure of the initial nucleus is changed, when many nucleons are removed. If, for instance, half the nucleus is cut away, it is meaningless to evaluate its excitation energy by considering holes in the initial Fermi distribution.

Therefore, the estimates of the prefragment excitation energy obtained by considering holes in the initial Fermi distribution should be taken with caution. In Refs. [19–21] this is already demonstrated at intermediate energies $\sim 1A$ GeV. As found by the comparison of the abrasion-ablation model predictions based on Eq. (13) with experimental data, the average excitation energy induced by the abrasion process should amount to 27 MeV per abraded nucleon in order to better describe the data. The additional excitation was attributed to final state interaction. In Ref. [21], particularly, the excitation-energy distributions given by Eq. (13) were stretched by a factor of 1.5–1.8 for a better description of fragment production cross sections for different elements.

On the other hand, one may expect that the model works better for high energy heavy ion collisions compared with intermediate energies of $\sim 0.1-1\ A$ GeV. Indeed, in the latter case, the momenta of recoil nucleons may be comparable to the momenta of intranuclear nucleons and their angular distribution is very wide so that they can be easily captured by one of the spectators. The situation changes at high energies, where the transverse momenta of knocked-out nucleons are typically large, ~ 0.5 GeV/c [27], and their subsequent capture is less probable. Other physical effects such as a finite hadronization length may further reduce the interaction probability of secondary hadrons produced in primary *NN* collisions.

In the present paper we try to verify the validity of the abrasion-ablation model at higher energies. Rather than introduce empirical excitation-energy enhancement factors, we invoke both Eqs. (13) and (14) in calculations. In view of the fact that these expressions give very different average excitations, our calculations cover the range of excitation energies considered in the early studies [19–21] with and without empirical enhancement of excitation energy of prefragments.

3. Empirical parametrization for prefragment excitation energy

Multifragmentation of spectators in ^{197}Au collisions with C, Al, Cu, and Pb targets at 600*A* GeV has been studied by the ALADIN Collaboration [28]. Such a study was specially aimed at those peripheral collisions where high excitation energies were deposited in the spectators. This leads to multifragment decay of hot nuclear systems. The comprehensive data on the cross sections of multifragment processes, on the neutron-to-proton ratios of produced fragments, on the differential distributions of fragment multiplicities, and on the

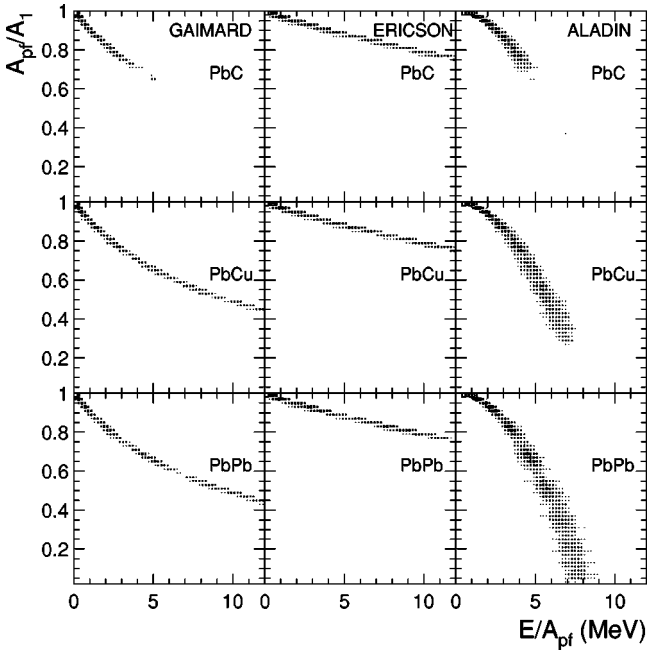

FIG. 6. Correlation between excitation energy per nucleon of prefragment, E/A_{pf}, and its relative mass, A_{pf}/A_1, for 158*A* GeV Pb ions on C, Cu, and Pb targets. Results for the Gaimard-Schmidt formula with $g_0=16$ MeV^{-1}, $g_1=0.4$ MeV^{-2} and the Ericson formula for $E_{max}=40$ MeV are given in the first and second columns, respectively. The same correlation based on the empirical parametrization of Ref. [28] is given in the third column.

charge correlations within each event are well described by SMM [18].

From the best fit to experimental data obtained by the ALADIN collaboration for AuCu collisions, the correlation between the average prefragment excitation energy per nucleon and its average relative mass was found to be [28]

$$\frac{\langle A_{pf}\rangle}{A_1} = 1 - 0.015\left(\frac{E}{A_{pf}}\right)^2, \tag{15}$$

where E is expressed in MeV. Gaussian distributions of A_{pf} around their mean values were assumed. Such correlation is shown in Fig. 6 along with the same correlations obtained for the Gaimard-Schmidt and Ericson formulas. It should be remembered that the parametrization given by Eq. (15) is specific for the investigated AuCu reaction at 600*A* MeV, and the mass and charge distributions of prefragments suggested in Ref. [28] differ from the corresponding distributions given by the abrasion model.

4. Comparison of excitation energy of prefragments calculated by different approaches

The average excitation energy per prefragment nucleon, $\langle E\rangle/A_{pf}$, can be expressed as a function of the number of removed nucleons a. This makes the difference between the abrasion approach and the ALADIN parametrization more transparent. For the abrasion model we obtain:

$$\frac{\langle E\rangle}{A_1 - a} = \mathsf{k}\frac{a}{A_1 - a}, \tag{16}$$

with $\mathsf{k}\sim 10-40$ MeV. This expression is divergent at $a \to A_1$, and both the Gaimard-Schmidt and Ericson approaches do not show any limitation of E/A_{pf} at large a. A large number of holes created in a prefragment will lead to excitation energies even exceeding its binding energy.

On the other hand, one may expect that a prefragment exists as a bound system only if its excitation energy is limited, $E/A_{pf} \lesssim 8$ MeV. This is reflected in the ALADIN parametrization:

$$\frac{\langle E\rangle}{A_1 - a} = \epsilon_{max}\left(\frac{a}{A_1}\right)^{1/2}, \tag{17}$$

which tends to the saturate at $\epsilon_{max}\approx 8$ for $a \to A_1$. The discussed difference in correlations between E and A_{pf} given by the abrasion model, Eq. (16), and the ALADIN parametrization, Eq. (17), is clearly seen in Fig. 6.

The Gaimard-Schmidt formula, Eq. (13), the Ericson formula, Eq. (14), and the empirical ALADIN parametrization, Eq. (15), serve as complementary approaches. The excitation energy estimates based on the densities of holes are expected to be not well grounded for large numbers of holes and high excitation energies. In contrast, the ALADIN parametrization was found from the analysis of multifragmentation events, which represent collisions leading to high excitation energies. Since these approaches are aimed at different domains of E and A_{pf}, it is important to understand their relations and find ways to extrapolate the parametrizations to high and low excitation energies.

Although these excitation energy trends clearly differ, difficulties emerge when the proper choice of one of these approaches should be made on the basis of the comparison of the calculated cross sections $\sigma(A,Z)$ given by Eq. (10) and experimental data. Since the integration over E and the sum over A_{pf}, Z_{pf} and decay channels i of prefragments appear in Eq. (10), the resulting cross section is indirectly influenced by the actual shape of excitation energy distribution used in calculation. The branching ratios of prefragment decay channels are also complicated functions of E.

However, depending on the masses of colliding nuclei a crucial test of the model is provided by the comparison with experimental data to a greater or lesser extent. We expect that the case of asymmetric PbC collisions is more sensitive to the choice of the E dependence compared to the case of symmetric PbPb collisions. Indeed, in collisions of lead nuclei with light targets, only relatively heavy prefragments with $A_{pf}/A_1 > 0.6$ can be created in the abrasion step, as shown in Fig. 6. With this restriction it is more safe to evaluate prefragment excitation energy by considering holes in the initial Fermi distribution, and a natural limitation is imposed on E in this case. Particularly, if E exceeds the multifragmentation threshold, intermediate-mass fragments have their origin in the ablation step only due to the decay of a heavy prefragment.

In Fig. 7 prefragment mass distributions are given separately for low ($E/A_{pf} < 2$ MeV) and high ($E/A_{pf} > 4$ MeV)

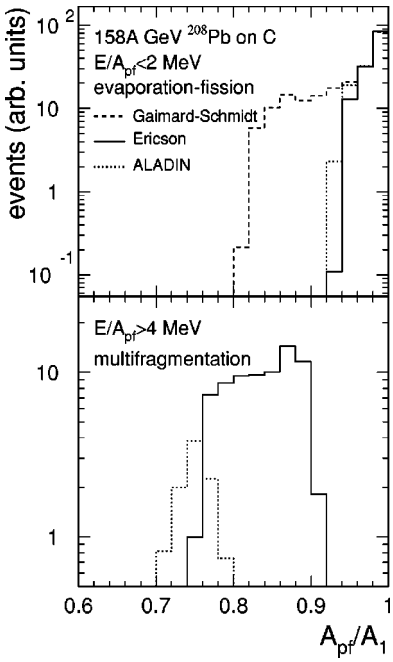

FIG. 7. Mass distributions of excited prefragments (arbitrary units) produced in 158*A* GeV PbC collisions after the abrasion step. Prefragment distributions calculated by the Gaimard-Schmidt formula, the Ericson formula, and the ALADIN parametrization, are given by the dashed, solid, and dotted histograms, respectively. Top panel: prefragments with $E/A_{pf}<2$ MeV, which undergo decay via evaporation-fission competition. Bottom panel: highly excited prefragments with $E/A_{pf}>4$ MeV, which undergo explosive multifragment breakup.

excitation energies for asymmetric PbC collisions. As will be discussed in Sec. III A 5, these two domains of E/A_{pf} correspond to evaporation-fission competition and mutifragmentation decays, respectively. The calculations based on the Ericson formula and the ALADIN parametrization give very similar distributions for $E/A_{pf}<2$ MeV, while by using the Gaimard-Schmidt formula a wider mass distribution is obtained. The distributions in the domain of multifragmentation ($E/A_{pf}>4$ MeV) are very different for each of the three cases. Of particular interest is the result that the Gaimard-Schmidt formula gives a negligible rate of multifragmentation events in PbC collisions (see Fig. 7). It can be tested by confronting this prediction with data, as will be performed in Sec. IV B.

The analysis of symmetric PbPb collisions is more complicated. First, light prefragments $A_{pf}/A_1<0.5$ can be directly produced in central collisions in the abrasion step, Fig. 6, and the concept of E estimated via hole energies becomes doubtful for these prefragments. Second, the presence of intermediate-mass fragments among reaction products cannot be considered as a clear sign of E/A_{pf} exceeding the multifragmentation threshold. Intermediate-mass fragments can be also directly created by abrasion in addition to their production via the decay of excited prefragments in the ablation step.

5. Description of prefragment decay

The decay of prefragments is described by the SMM [18]. According to this model, the decay mode of an excited prefragment A_{pf} is determined by its excitation energy per nucleon E/A_{pf}. For $E/A_{pf}<2$ MeV, the deexcitation proceeds via successive emission of particles (evaporation) or fission. When the excitation energy exceeds about half the prefragment total binding energy ($E/A_{pf}>4$ MeV), the explosive multifragment breakup dominates. In the transition region ($2\lesssim E/A_{pf}\lesssim$MeV) both decay processes coexist. At $E/A_{pf}>10$ MeV the prefragment breaks up into nucleons and lightest clusters (vaporization). Therefore, depending on E/A_{pf}, an excited prefragment exists either in the form of a compound nucleus, or as a system of unbound nucleons.

As the full description of the SMM model was given in Ref. [18], we briefly summarize here only the main points of our approach to describe different decay mechanisms for given E, A_{pf}, and Z_{pf}. The simulation of the prefragment decay process is performed by the Monte Carlo method.

Evaporation of nucleons and light nuclei from an excited prefragment is described by the standard Weisskopf evaporation scheme. The calculation of the partial width Γ_j for the evaporation of a particle j (where j represents n,p,d,t, ^{3}He, α, or light nuclei up to oxygen) is based on the cross section for the inverse capture reaction of the particle j to form the prefragment (compound nucleus) times the ratio of the nuclear level densities for the initial and final nuclei [17,29]. The nuclear level densities are calculated according to the Bethe formula [30] for the equispaced model with the level density parameter extracted from approximations to experimental data.

The Bohr-Wheeler statistical approach [31] was originally used in the SMM model [18] to calculate the fission width Γ_f^{BW} of a prefragment. The ratio of the nuclear level densities at the fission saddle point and in the initial prefragment is a key quantity in such calculations. However, as found in experiments (see Ref. [32] as an example), the fission probability grows much less rapidly with increasing excitation energy than one would expect from the Bohr-Wheeler formula. A diffusion model approach based on the solution of a Fokker-Planck equation for the distribution function of a fission variable was developed in Refs. [33,34]. It was found that a certain transient time τ is needed for the system to build up the quasistationary probability flow over the fission barrier. The larger the τ, the more particles are evaporated during the transition time, thus reducing the prefragment excitation energy. As a consequence, the evaporation-fission competition leads to a reduction in the effective fission probability $\Gamma_f=\Gamma_f^{BW}K$, with $K<1$. A detailed study of dissipation in the fission process was given recently in Ref. [32] for the reaction of 800*A* MeV ^{197}Au on protons. Several values of the dissipation coefficient β and functional forms for the time-dependent fission probability $\Gamma_f(t)$ were used to reproduce the fission data.

In the present work we are dealing with inclusive data where fission and fragmentation contributions are not separated. Therefore, we treat fission in competition with other fragmentation channels. The correction factor K to the Bohr-Wheeler formula was found from a fit to the data yielding $K\sim 0.3$, (see Sec. IV). Also a lower limit for the lifetime of a fissioning nucleus, $\tau_f=\hbar/\Gamma_f\gtrsim 10^{-20}$ s, was introduced in the SMM model, keeping in mind that τ_f should certainly exceed the transient time $\tau\sim 3\times 10^{-21}$ s found in Ref. [32].

At sufficiently high excitation energy, $E/A_{pf} \gtrsim 2$ MeV, the explosive multifragment breakup becomes important. According to the SMM, a highly excited prefragment expands to a "freeze-out" volume where it splits into primary hot fragments and nucleons in thermal equilibrium. The breakup channels are constrained by the total mass, charge, and energy of the system. It is assumed that the probabilities of different breakup channels are proportional to their statistical weights. After primary breakup, excited fragments propagate independently under their mutual Coulomb repulsion and undergo secondary decays described by evaporation, Fermi breakup or fission depending on their masses and excitation energies (see Refs. [17,18] for details). As shown by numerous analyses [18,28,35], the SMM provides a very good description of spectator fragmentation in nucleus-nucleus collisions.

B. Charge-changing reactions due to electromagnetic interactions

An ultrarelativistic projectile with Lorentz factor $\gamma \gg 1$ may be also torn apart by long-range electromagnetic forces in addition to the abrasion-ablation process due to strong interactions considered in Sec. III A. Ultraperipheral heavy-ion collisions without direct overlap of nuclear densities can be described within the Weizsäcker-Williams (WW) method of equivalent (virtual) photons [36–38]. These photons induce subsequent photonuclear reactions (γA) leading to so-called electromagnetic dissociation (ED) of nuclei with emission of protons among other possible disintegration products [39]. Since the flux of equivalent photons, as seen by a projectile, is proportional to the square of the target charge, one can expect an important contribution to the charge-changing cross section for medium and heavy target nuclei.

1. Charge loss in electromagnetic dissociation

A detailed description of the RELDIS model used to describe ED processes was given in Refs. [7,40]. The calculations are based on the WW method taking into account single and double photon absorption of equivalent photons. Double photon absorption processes are taken into account by applying the harmonic-oscillator ansatz in combination with the folding model [41].

The convolution of the virtual photon spectrum with the total photoabsorption cross section $\sigma_{A_1}(E_\gamma)N(E_\gamma)$, which appears to be a key ingredient of the calculation, is plotted in Fig. 8. Here, $\sigma_{A_1}(E_\gamma)$ is the total photoabsorption cross section for the projectile nucleus A_1, and $N(E_\gamma)$ is the virtual photon spectrum as seen by the projectile.

Depending on the virtual photon energy E_γ, different processes may contribute to nuclear disintegration which is observed in the present experiment as a charge loss of the projectile. When a ^{208}Pb nucleus absorbs one or two virtual photons in the giant dipole resonance (GDR) region, $6 \leqslant E_\gamma \leqslant 30$ MeV, their energies are completely transformed into nuclear excitation energy E. Since ^{208}Pb has a high fission threshold, its deexcitation proceeds mainly through the evaporation of neutrons with separation energies only around

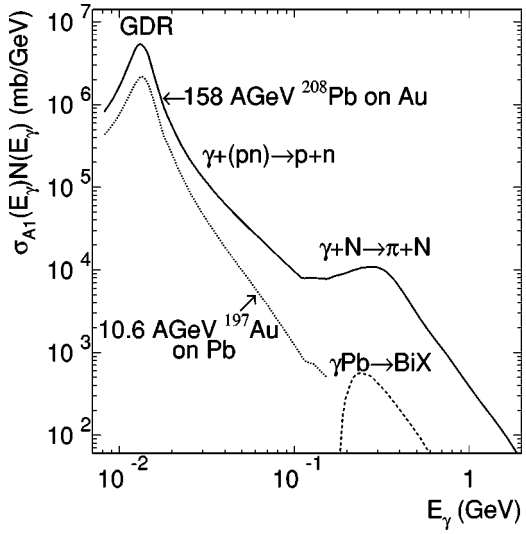

FIG. 8. Product of the virtual photon spectrum and the total photoabsorption cross section used in RELDIS calculations for 10.6*A* GeV Au ions (dotted line) and for 158*A* GeV Pb ions (solid line). The domains of photoabsorption via GDR excitation, quasideuteron mechanism, and Δ excitation are shown. The product of the $_{83}$Bi photoproduction cross section and the virtual photon spectrum for 158*A* GeV ions is shown by the dashed line.

7 MeV. Due to a high Coulomb barrier, proton emission is suppressed in the GDR region.

Proton emission in the γPb process begins at $E_\gamma \geqslant 40$ MeV, when the quasideuteron absorption, $\gamma + (np) \rightarrow n + p$, becomes important, and a fast proton has a high probability to escape. Above the single-pion production threshold at $E_\gamma = 140$ MeV the photoabsorption on a single nucleon is possible via the $\gamma N \rightarrow \pi N$ reaction, mainly by Δ resonance excitation. Finally, multiple-pion production comes into play above the Δ-resonance region. In all cases, the emission of protons in primary and secondary interactions is taken into account by the intranuclear cascade model of photonuclear reactions [42]. In this model, the initial γN interaction induced by an equivalent photon initiates a cascade of successive quasifree hadron-nucleon collisions in the nucleus. As a result, an excited residual nucleus is formed after the cascade stage. Its decay is again described by the SMM (see Sec. III A 5), but compared to hadronic reactions the excitation energy deposited by virtual photons is much lower on average [40]. Therefore, mainly proton evaporation and possibly fission channels contribute significantly to charge-loss interactions of Pb projectiles in ultraperipheral collisions.

The maximum equivalent photon energy is estimated as $E_{\max} = \gamma \hbar c / b_c$, where b_c is the minimum impact parameter in the electromagnetic interaction, Eq. (2). In the case of 158*A* GeV Pb projectiles, $E_{\max}$ amounts to 4.1 GeV for Pb + H and to 2.2 GeV for Pb + Au collisions. These values are much larger than the pion production threshold on a free nucleon, $E_{th} \simeq 140$ MeV, and the whole set of processes described above has to be taken into account. This is done in a systematic way by the RELDIS code.

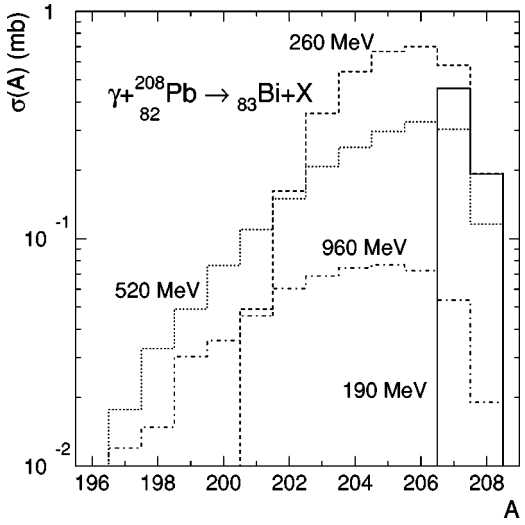

FIG. 9. Cross sections for photoproduction of $^{A}_{83}$Bi isotopes by monoenergetic photons on ^{208}Pb as predicted by the RELDIS model. The results for photon energies of $E_\gamma = 190, 260, 520$, and 960 MeV are shown by the solid, dashed, dotted, and dash-dotted lines, respectively.

2. Charge pickup in electromagnetic dissociation

At ultrarelativistic energies ($\gamma \gtrsim 100$), a new mechanism of nuclear-charge-changing interactions comes into play because the maximum equivalent photon energy in electromagnetic interactions exceeds the pion production threshold [43]. Dominant processes lead to a *reduction* in projectile charge Z_1 via proton loss or emission of π^+ mesons. In rare cases, however, the nuclear charge of the projectile is *increased*. We term such a process electromagnetically induced nuclear charge pickup ($\Delta Z = +1$).

A π^- produced in the reaction $\gamma n \to \pi^- p$ may be emitted, while the associated proton can be captured to form a $(Z_1 + 1)$ residual nucleus. In general, this nucleus is excited. In most cases, however, deexcitation involves only neutron evaporation. This is illustrated in Fig. 9, where the calculated cross sections to produce different Bi isotopes by monoenergetic photons impinging on ^{208}Pb are shown. If a photon close to the threshold energy is absorbed, $E_\gamma = 190$ MeV as an example, the nucleus obtains a low excitation energy. In some cases only π^- is emitted. We assumed an attractive potential of $V_\pi \simeq 35$ MeV for negative pions inside the nucleus, and therefore pion emission starts above the free-nucleon threshold E_{th}. In contrast, at $E_\gamma = 520$ MeV, many more neutrons are evaporated, leading to much more neutron-deficient residual Bi isotopes.

According to our calculations, the cross section to produce Bi in γPb reactions does not exceed 4% of the total photoabsorption cross section. As shown in Fig. 8, the contribution of the $\gamma\mathrm{Pb} \to \mathrm{Bi}X$ reaction is noticeable in the range of photon energies of $E_\gamma = 200-600$ MeV. Photonuclear reactions of the type $(\gamma, \pi^- xn)$, $x = 0, \ldots, 9$, induced by *real* bremsstrahlung photons, were studied some years ago and the reader is referred to a recent paper where such reactions were studied by radiochemical methods [44]. Analogous reactions, induced by *equivalent* photons, are possible in ultrarelativistic heavy-ion collisions.

IV. COMPARISON OF THEORY AND EXPERIMENT

A. Total charge-changing cross section

The most integral characteristic of charge-changing reactions is the total charge-changing cross section, σ_{cc}. It can be easily calculated as the difference between the total reaction cross section and the cross section for fragmentation with only neutron emission:

$$\sigma_{cc} = \sigma_R - \sum_A \sigma(A, Z = 82) + \sigma^{ED}(\mathrm{tot}) - \sum_A \sigma^{ED}(A, Z = 82). \tag{18}$$

Here the total reaction cross section σ_R is calculated as πb_c^2 with b_c given by the BCV formula, Eq. (2), and $\sigma(A,Z)$ is calculated according to Eq. (10). The superscript ED stands for the corresponding values in electromagnetic interactions calculated by the RELDIS model.

Theoretical results for σ_{cc} are plotted in Fig. 4 for nuclear and electromagnetic contributions. Their sum describes our experimental data quite well.

The hadronic contribution to σ_{cc} is obtained by subtracting a small part of $\sim(0.47-0.63)$ b of mostly peripheral ($\Delta Z = 0$) reactions from the total hadronic cross section of $\sim(2.0-7.4)$ b, depending on the target mass from hydrogen to lead. Therefore, σ_R for hadronic interactions can be well approximated by the corresponding σ_{cc}. In contrast, $\Delta Z = 0$ reactions constitute a *major* part ($\sim 85-90\%$) of the total ED cross sections at 158*A* GeV. This is explained by a dominant contribution of GDR excitation followed by subsequent neutron emission. The measured data can be explained on the basis of the present models and do not show any peculiar behavior, which could explain the enhancement mentioned in Ref. [45], the origin of which remains still unknown.

B. Partial charge-changing cross sections

Calculation results for hadronic and electromagnetic contributions to charge-loss cross sections for 158*A* GeV ^{208}Pb projectiles are presented in Figs. 10–12, to be compared with our experimental data and the data of Refs. [3,6]. In addition, the results for fragmentation of 10.6*A* GeV ^{197}Au ions are given in Fig. 13 to be compared with the data of Ref. [46]. Since we do not expect the abrasion-ablation model to work for Pb fragmentation on H, the calculations for this case are not presented. In particular, one cannot simply extrapolate to the $A_2 = 1$ case the nuclear density and thickness functions, Eqs. (5) and (6). Also the experimental data for hydrogen have larger statistical uncertainties, since they are obtained as a difference between the measurements on polyethylene and carbon.

The methods of calculating excitation energies of prefragments via the hole state densities given in Sec. III A 2, or via the empirical parametrization, Sec. III A 3, should be merely considered as model assumptions. To constrain the models, their predictions should be tested with experimental data for hadronic heavy-ion interactions.

Since measurements give the sum of hadronic and electromagnetic contributions, their relative weights can be obtained only by using specific models. As follows from the

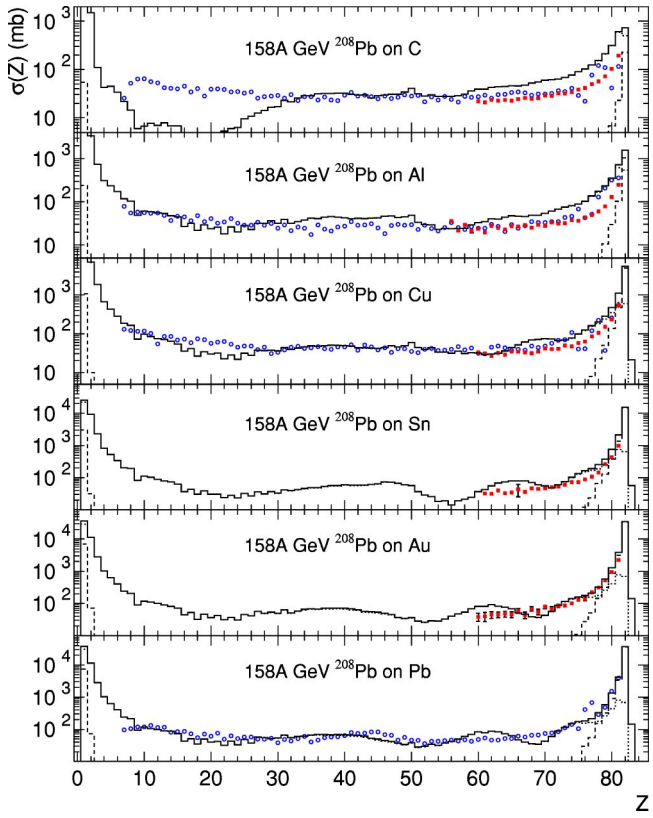

FIG. 10. (Color online) Inclusive cross sections for producing a fragment with charge Z by 158A GeV ^{208}Pb projectiles on C, Al, Cu, Sn, Au, and Pb targets. Experimental data are shown by the full squares (this work) and by the open circles (Refs. [3,6]). Results of calculations with the abrasion-ablation model with $\rho_a(E)$ given by the Gaimard-Schmidt formula, Eq. (13), with $g_0=16$ MeV^{-1}, $g_1=0.4$ MeV^{-2}, and with the RELDIS model are shown by the dotted and dashed histograms, respectively. The solid histograms represent their sums.

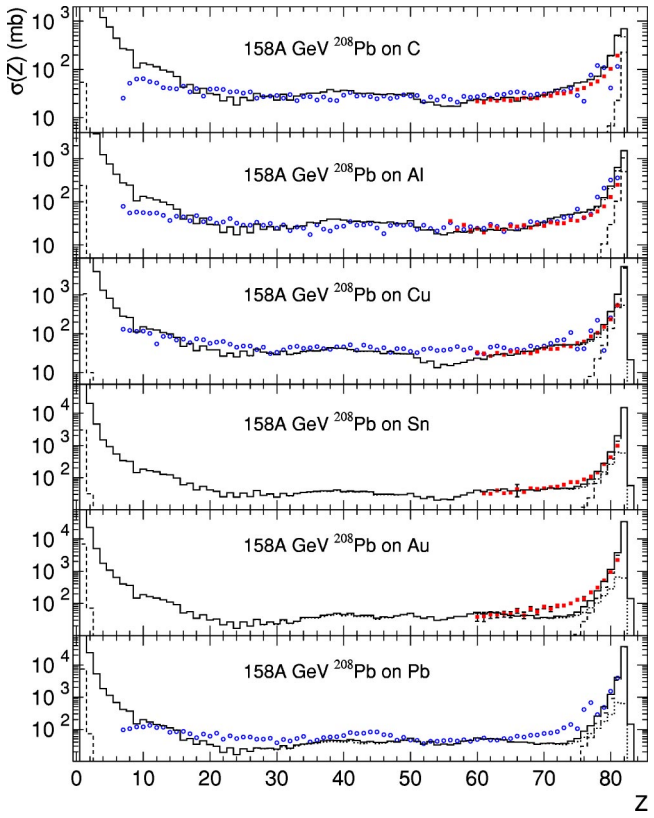

FIG. 11. (Color online) Same as Fig. 10, but for calculations made with $\rho_a(E)$ given by the Ericson formula, Eq. (14), and with a factor of $K=0.3$ used in fission calculations.

RELDIS model, electromagnetic contributions to fragmentation of 158A GeV Pb ions are significant only for $-3\leqslant\Delta Z\leqslant-1$. Figure 10 shows that this contribution is comparable to the hadronic contributions for Cu and Sn targets, and is dominating for Au and Pb targets.

Electromagnetic contributions are less important at the lower energy of 10.6A GeV (Fig. 13), but even there, about 50% of the one-proton loss on a Pb target is due to electromagnetic interactions. Unfortunately, experimental data are not available for $\Delta Z=0$ channels with only neutrons emitted, but we expect electromagnetic contributions to dominate in these channels at $\sim$10–100 A GeV on medium-weight and heavy targets.

After the electromagnetic contribution is well established, we can concentrate our attention on the hadronic fragmentation. Two remarks should be made on calculation results obtained with the Gaimard-Schmidt formula (Fig. 10). First, the production of intermediate-mass fragments, $7\leqslant Z\leqslant30$, is underestimated in PbC collisions. As demonstrated in Sec. III A 4, intermediate-mass fragments are expected to be produced via multifragment decays of heavy prefragments in the case of asymmetric PbC collisions, but apparently the rate of such events is underestimated by the model. Second, the model overestimates the production of heavy fragments, $60\leqslant Z\leqslant81$, in PbC, PbAl, and PbCu collisions. Such fragments are produced by evaporating protons and neutrons, and apparently the evaporation chains were not sufficiently long. Both observations indicate that prefragment excitation energies are too low when the Gaimard-Schmidt formula is used to calculate excitation energy of prefragments in high-energy heavy-ion collisions. As mentioned in Sec. III A 2, with the parameters used in the calculation ($g_0=16$ MeV^{-1} and $g_1=0.4$ MeV^{-2}) it gives $\sim$13 MeV average excitation for the first removed nucleon and $\sim$8–10 MeV for subsequent nucleons.

It is expected that a better description of the data will be obtained with the Ericson formula, which gives higher excitation energies of prefragments. Indeed, the Ericson formula gives $\sim$20 MeV average excitation per hole for the first nucleon removed and $\sim$40 MeV for subsequent nucleons. Figure 11 confirms this expectation. Here, the cross sections for light ($7\leqslant Z\leqslant30$) and heavy ($60\leqslant Z\leqslant81$) fragments are in much better agreement with the data. The quality of description of experimental results was found reasonable for light, medium-weight, and heavy targets. In order to describe better the production of fission fragments, $Z\sim30$–50, we used a correction factor of $K=0.3$ in the Bohr-Wheeler formula. We believe that more sophisticated fission models, e.g., of Refs. [33,34], should be used for high E instead of the Bohr-Wheeler statistical approach.

Choosing between the Gaimard-Schmidt and Ericson formulas for $\rho_a(E)$, one should keep in mind that this distribu-

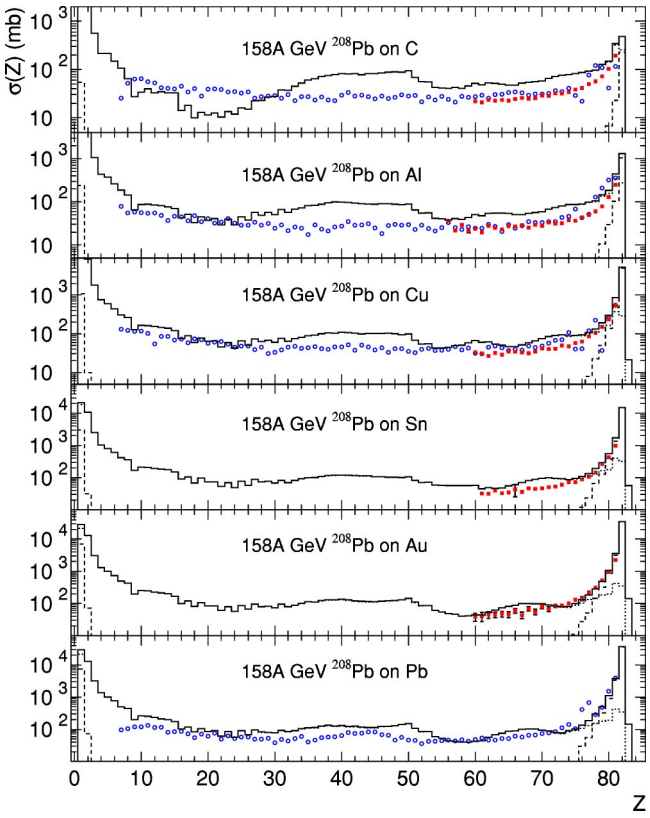

FIG. 12. (Color online) Same as in Fig. 11, but for the calculations made with prefragment excitation energy E estimated from ALADIN data [28].

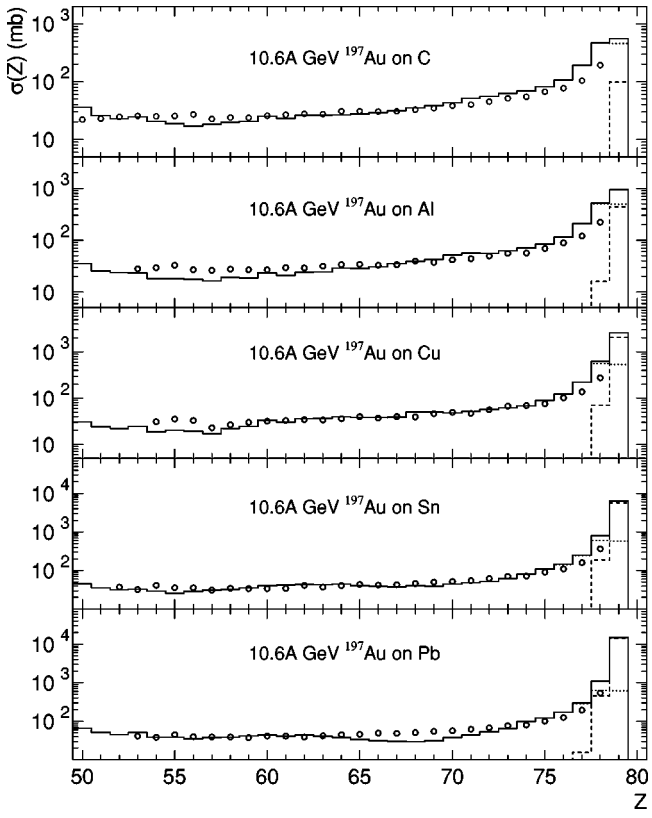

FIG. 13. Inclusive cross sections for producing a fragment with charge Z by 10.6A GeV ^{197}Au projectiles on C, Al, Cu, Sn, and Pb targets. Experimental data are shown by the open circles [46]. Calculations were made with $\rho_a(E)$ given by the Ericson formula, Eq. (14), and with a factor of $K=0.3$ used in fission calculations. Other notations are the same as in Fig. 10.

tion may, in principle, implicitly account for production of secondary hadrons, increasing the prefragment excitation energy E. As mentioned in Sec. III A 2, these hadrons may create additional holes in the primary nucleus. In this way, the exact correlation between E and the number of holes created after *primary removal* of nucleons is destroyed. Therefore, $\rho_a(E)$ presents the amount of energy delivered to a prefragment not only due to removal of a nucleons in *primary NN collisions*, but also due to possible *secondary hadronic interactions*.

Finally, the ALADIN parametrization was also tested with results given in Fig. 12. Our results confirm its validity for the intermediate-mass fragment production, $7 \leqslant Z \leqslant 30$, in PbAl, PbCu, and PbPb collisions, but show poor description of light fragments in PbC collisions. In this set of calculations based on the ALADIN parametrization we have used the same correction factor $K=0.3$, but the model clearly overestimates the production of fission fragments on most of the targets. The production of heavy fragments, $60 \leqslant Z \leqslant 81$, is overestimated as well. It should be reminded that the ALADIN parametrization was obtained in Ref. [28] to describe the data on Au fragmentation on Cu at 600A MeV. It is based on the analysis of more detailed experimental data on fragment production compared to the inclusive charge-changing cross sections of the present work. All three approaches were tested with 10.6A GeV Au data [46], available for heavy fragments ($50 \leqslant Z \leqslant 78$), and the best description was again found for the calculations based on the Ericson formula, as shown in Fig. 13.

In summary, the usefulness of abrasion-ablation model is justified for collisions of Pb and Au with light targets and for peripheral collisions with heavy- and medium-weight targets. The fact that excitation energy of prefragments is underestimated by the model can be revealed by the analysis of asymmetric PbC collisions, and, especially, by considering the production of intermediate-mass fragments, $3 \leqslant Z \leqslant 30$.

C. Charge-pickup reactions

Charge-pickup reactions can be easily explained at low collision energies, below the Fermi energy, by proton transfer from one collision partner to the other. At relativistic energies, however, the Fermi spheres of projectile and target are totally nonoverlapping, preventing any transfer of a target proton to the projectile. Instead, we can assume Δ-resonance formation and decay in NN collisions to be the most likely elementary processes in which a projectile neutron can be converted into a proton, e.g., by $n \rightarrow \Delta^0 \rightarrow p + \pi^-$ with subsequent absorption of the proton in the projectile and emission of the π^- [47] and, possibly, neutrons.

Systematic experimental studies of inclusive charge-pickup cross sections $\sigma(\Delta Z=+1)$ as functions of incident energy and target mass reveal a steady decrease of these cross sections with increasing energy, as shown in Fig. 14.

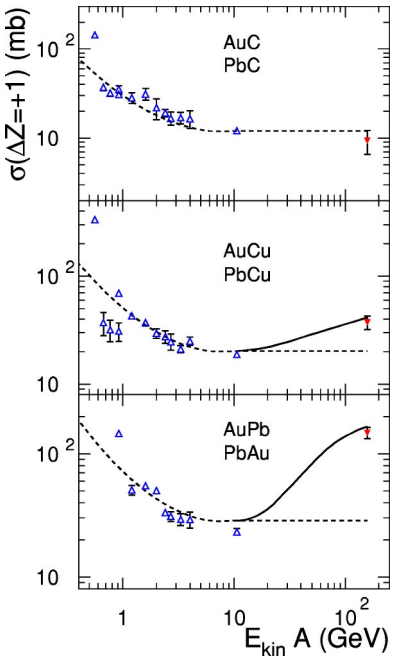

FIG. 14. (Color online) Energy dependence of charge-pickup cross sections for Au and Pb projectiles on C, Cu, Au, or Pb targets. Experimental data [46,48,49] for Au projectiles at 10.6*A* GeV and below are given by the open triangles, present data for Pb projectiles at 158*A* GeV by the full triangles. Fit results of Ref. [2] are given by the dashed lines. The solid lines represent the dashed curves plus an electromagnetic contribution calculated by the RELDIS model.

This holds for different projectiles with energies between 0.5*A* and 10*A* GeV [46,48,49].

The dependence on target mass A_2 is very weak and can be described by a power law $\sigma(\Delta Z=+1)\propto A_2^{\kappa}$ with an energy-independent exponent of $\kappa=0.223\pm0.005$ [49]. A steady decrease with bombarding energy was also reflected in fits of charge-pickup cross sections [2] based on (p,xn) cross sections modified for target dependence by an additional factor, $(Z_2/6)^{1/3}$. The fit is valid for heavy projectiles $(Z_1>50)$ with a weak target dependence for $Z_2\geqslant 6$. $\sigma(\Delta Z=+1)$ values were supposed to be constant above $\sim 4A$ GeV and they were extrapolated in such a way until $\sim 100A$ GeV [2]. These observations suggest that the $NN\rightarrow N\Delta$ reaction mentioned above is the most likely mechanism, and that electromagnetic processes do not contribute to $\sigma(\Delta Z=+1)$. The measurements of Dekhissi *et al.* [3] at 158*A* GeV yielded similar results, with a slightly increased exponent $\kappa=0.4\pm0.1$ for target dependence.

Our experimental results for 158*A* GeV Pb ions as well as their interpretation are drastically different. As discussed in Sec. III B 2, the electromagnetic contribution to the charge-pickup cross sections for ions with $\gamma\leqslant 10$ is almost negligible, since the highest possible equivalent photon energy is smaller than the pion-production threshold. The situation is completely different at 158*A* GeV, where a substantial part of the virtual photon spectrum exceeds this threshold. As one can see clearly in Fig. 8, the absorption of virtual photons via GDR excitation and quasideuteron absorption dominate in both cases, but, in addition, photon absorption in the Δ-resonance region becomes important for the higher beam energy.

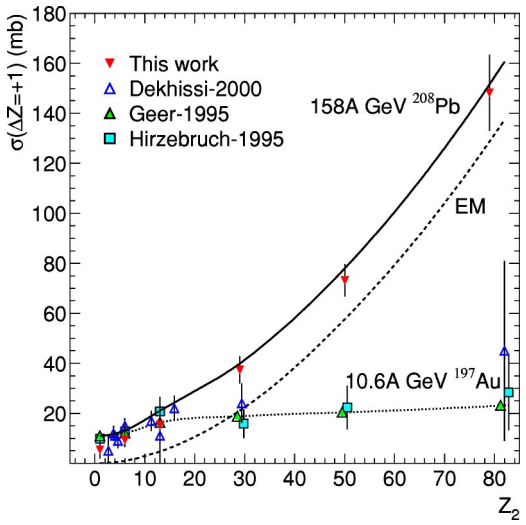

FIG. 15. (Color online) Nuclear-charge pickup $(\Delta Z=+1)$ cross sections as a function of target atomic number Z_2. The data for 158*A* GeV Pb ions are shown by the full (present work) and open triangles (Ref. [3]). The solid curve is the sum of the electromagnetic contribution (EM, dashed line) and the nuclear contribution to the $\Delta Z=+1$ cross section. For comparison, data obtained with 10.6*A* GeV Au ions [46,50] are depicted with the light-colored triangles and squares, which are connected by the dotted line to guide the eye.

The electromagnetically induced charge pickup originates exclusively from the latter part of the spectrum. The energy dependence of $\sigma(\Delta Z=+1)$ contribution is presented in Fig. 14. The total $(\Delta Z=+1)$ cross section decreases up to 10*A* GeV, but then it starts rising again due to opening of $\gamma N\rightarrow\pi N$ channels. This effect can be neglected only on very light targets such as carbon, where the electromagnetic contribution to $\sigma(\Delta Z=+1)$ is small, ~1 mb, and not shown in Fig. 14.

Our results for charge-pickup $(\Delta Z=+1)$ cross sections are shown in Fig. 15 as a function of the target charge Z_2. For a quantitative comparison with the experimental data we assume, following Ref. [2], that the *hadronic contribution* for 158*A* GeV Pb ions is identical with the charge-pickup cross section measured for 10.6*A* GeV Au ions [46] (the data of Ref. [50] are not used because of their much larger uncertainties). Thus adding the values of Ref. [46] to our theoretical predictions, we obtain the total charge-pickup cross sections $\sigma(\Delta Z=+1)$ visualized by the full line in Fig. 15. In particular, for medium-weight and heavy targets the results of the RELDIS calculation are in excellent agreement with the measured data. It should be noted that pure π and ρ exchange as described in Ref. [51] seems to be insufficient to describe our experimental findings.

V. CONCLUSIONS

New experimental data on charge-changing cross sections of 158*A* GeV ^{208}Pb ions on different targets were presented

along with their theoretical interpretation. Electromagnetic contributions to charge-loss reactions for $-3<\Delta Z<-1$ calculated within the RELDIS model were found comparable to hadronic contributions for Al target and even dominating for Cu, Sn, Au, and Pb targets.

In contrast to earlier studies performed at intermediate energies [48,49] and at 10.6*A* GeV [46,50], we observe a strong, almost quadratic increase of the nuclear-charge pickup ($\Delta Z=+1$) cross sections with target charge. Our experimental findings can be described quantitatively with RELDIS calculations showing that in collisions with high-*Z* nuclei the dominant contribution to nuclear-charge pickup is due to electromagnetic processes of π^- production by virtual photons. This contribution is completely negligible at Alternating Gradient Synchrotron (AGS) energies and is observed for the first time in the present experiment at the CERN SPS.

We found that production of nuclear fragments in peripheral or semiperipheral hadronic collisions of heavy nuclei at ultrarelativistic energies (with Lorentz factors of $\gamma\gtrsim 10$) may be described by the two-stage mechanism, that was proven in the past to be valid at intermediate energies ($\gamma\sim 1$) [12–14]. Within such a two-stage picture, the abrasion of nucleons from the projectile creates an excited prefragment that then undergoes decay in the second (ablation) step. The excitation energy *E* of a prefragment was assumed to be approximately proportional to the number of holes left by abraded nucleons in the primary nucleus. Historically [13,14,19,21], the ablation step in fragmentation of heavy projectiles like Au, Pb, or U was considered as a sequential decay process, proceeding through the evaporation-fission competition.

Our modified description of the ablation step removes an obvious deficiency of the traditional model: if a relatively large number ($\gtrsim 20-30\%$) of projectile nucleons is removed, the excitation energy *E* exceeds the total binding energy of a prefragment. This makes it impossible to apply a sequential evaporation-fission decay mechanism, which is based on the concept of the compound nucleus as an excited, but still bound system. According to the SMM employed in the present work, when the excitation energy exceeds about half the prefragment total binding energy, the system decays mainly via explosive multifragment breakup. Indications for a simultaneous break-up process were also recently highlighted in Ref. [52] by comparison of abrasion-ablation calculations with experimental data for UPb collisions at 1*A* GeV.

The estimation of *E* via the hole state density in the projectile nucleus remains poorly justified for violent collisions with many nucleons removed. Nevertheless, it gives realistic predictions for charge-changing cross sections, which we compared to the experimental data for Au and Pb fragmentation on C, Al, Cu, Sn, Au, and Pb targets. The extrapolation of such an approach widely used at $\sim$1*A* GeV to ultrarelativistic energies seems to be surprisingly successful, especially in a view of the fact that secondary hadrons are copiously produced in *NN* collisions at such energies.

We found that the excitation energy deposited in prefragments may on average amount to $\sim$40 MeV per removed nucleon, in good agreement with the Ericson formula. This value is higher than the value of $\sim$27 MeV found for Au fragmentation on Be at 950*A* MeV [19,21]. Such a difference may be attributed to additional heating of prefragments by secondary hadrons.

ACKNOWLEDGMENTS

We are indebted to G. Baur, P. Braun-Munzinger, and W. Trautmann for interesting discussions. Special thanks are due to E. Berdermann and H. Stelzer for help with the data acquisition. Several authors (H.F.K., C.R.V., S.D.) gratefully acknowledge support by U.S. DOE, Office of Basic Energy Sciences, Division of Chemical Sciences, under Contract No. DE-AC05-00OR22725 with UT-Batelle, LLC. H.K., U.U., and R.H.S. acknowledge the support of the Danish and Swedish Natural Science Research Councils. I.A.P. thanks GSI, NBI, and ENEA for the warm hospitality. I.N.M. thanks DAAD, Germany for financial support. This work was partly supported by the Russian Foundation for Basic Research, Grant Nos. 02-02-16013 and 03-02-04007.

[1] D. E. Greiner, H. Crawford, P. J. Lindstrom, J. M. Kidd, D. L. Olson, W. Schimmerling, and T. J. M. Symons, Phys. Rev. C **31**, 416 (1985).

[2] C. H. Tsao, R. Silberberg, and A. F. Barghouty, Astrophys. J. **501**, 920 (1998).

[3] H. Dekhissi, G. Giacomelli, M. Giorgini, G. Mandrioli, S. Manzoor, L. Patrizii, V. Popa, P. Serra, and V. Togo, Nucl. Phys. **A662**, 207 (2000).

[4] G. Hüntrup, T. Streibel, and W. Heinrich, Phys. Rev. C **61**, 034903 (2000).

[5] C. Scheidenberger, I. A. Pshenichnov, T. Aumann, S. Datz, K. Sümmerer, J. P. Bondorf, D. Boutin, H. Geissel, P. Grafström, H. Knudsen, H. F. Krause, B. Lommel, S. P. Moller, G. Münzenberg, R. H. Schuch, E. Uggerhoj, U. Uggerhoj, C. R. Vane, A. Ventura, Z. Z. Vilakazi, and H. Weick, Phys. Rev. Lett. **88**, 042301 (2002).

[6] S. Cecchini, G. Giacomelli, M. Giorgini, G. Mandrioli, L. Patrizii, V. Popa, P. Serra, G. Sirri, and M. Spurio, Nucl. Phys. **A707**, 513 (2002).

[7] I. A. Pshenichnov, J. P. Bondorf, I. N. Mishustin, A. Ventura, and S. Masetti, Phys. Rev. C **64**, 024903 (2001).

[8] M. Pfützner, H. Geissel, G. Münzenberg, F. Nickel, C. Scheidenberger, K. H. Schmidt, K. Sümmerer, T. Brohm, B. Voss, and H. Bichsel, Nucl. Instrum. Methods Phys. Res. B **86**, 213 (1994).

[9] H. Stelzer, Nucl. Instrum. Methods Phys. Res. A **310**, 562 (1991).

[10] H. F. Krause, C. R. Vane, S. Datz, P. Grafström, H. Knudsen, U. Mikkelsen, C. Scheidenberger, R. H. Schuch, and Z. Vilakazi, Phys. Rev. A **63**, 032711 (2001).

[11] C. J. Benesh, B. C. Cook, and J. P. Vary, Phys. Rev. C **40**, 1198 (1989).

[12] J. Hüfner, K. Schäfer, and B. Schürmann, Phys. Rev. C **12**, 1888 (1975).
[13] L. F. Oliveira, R. Donangelo, and J. O. Rasmussen, Phys. Rev. C **19**, 826 (1979).
[14] J.-J. Gaimard and K. H. Schmidt, Nucl. Phys. **A531**, 709 (1991).
[15] J. P. Bondorf, R. Donangelo, I. N. Mishustin, C. J. Pethick, H. Schulz, and K. Sneppen, Nucl. Phys. **A443**, 321 (1985).
[16] A. S. Botvina, A. S. Ilinov, and I. N. Mishustin, Yad. Fiz. **42** 1127 (1985) [Sov. J. Nucl. Phys. **42**, 712 (1985)].
[17] A. S. Botvina, A. S. Iljinov, I. N. Mishustin, J. P. Bondorf, R. Donangelo, and K. Sneppen, Nucl. Phys. **A475**, 663 (1987).
[18] J. P. Bondorf, A. S. Botvina, A. S. Iljinov, I. N. Mishustin, and K. Sneppen, Phys. Rep. **257**, 133 (1995).
[19] K.-H. Schmidt, T. Brohm, H. G. Clerc, M. Dornik, M. Fauerbach, H. Geissel, A. Grewe, E. Hanelt, A. Junghans, A. Magel, W. Morawek, G. Münzenberg, F. Nickel, M. Pfützner, C. Scheidenberger, K. Sümmerer, D. Vieira, B. Voss, and C. Ziegler, Phys. Lett. B **300**, 313 (1993).
[20] M. de Jong, K.-H. Schmidt, B. Blank, C. Böckstiegel, T. Brohm, H.-G. Clerc, S. Czajkowski, M. Dornik, H. Geissel, A. Grewe, E. Hanelt, A. Heinz, H. Irnich, A. R. Junghans, A. Magel, G. Münzenberg, F. Nickel, M. Pfützner, A. Piechaczek, C. Scheidenberger, W. Schwab, S. Steinhäuser, K. Sümmerer, W. Trinder, B. Voss, and C. Ziegler, Nucl. Phys. **A628**, 479 (1998).
[21] J. Benlliure, K. H. Schmidt, D. Cortina-Gil, T. Enqvist, F. Farget, A. Heinz, A. R. Junghans, J. Pereira, and J. Taieb, Nucl. Phys. **A660**, 87 (1999).
[22] J. C. Hill, A. Petridis, B. Falem, and F. K. Wohn, Nucl. Phys. **A661**, 313c (1999).
[23] K. H. Schmidt, H. Delagrange, J. P. Dufour, N. Carjan, and A. Fleury, Z. Phys. A **308**, 215 (1982).
[24] T. Ericson, Adv. Phys. **9**, 425 (1960).
[25] A. Harangozo, I. Stetcu, M. Avrigeanu, and V. Avrigeanu, Phys. Rev. C **58**, 295 (1998).
[26] M. Avrigeanu and V. Avrigeanu, Comput. Phys. Commun. **112**, 191 (1998).
[27] P. Senger and H. Strobele, J. Phys. G **25**, R59 (1999).
[28] A. S. Botvina, I. N. Mishustin, M. Begemann-Blaich, J. Hubele, G. Imme, I. Iori, P. Kreutz, G. J. Kunde, W. D. Kunze, V. Lindenstruth, U. Lynen, A. Moroni, W. F. J. Muller, C. A. Ogilvie, J. Pochodzalla, G. Raciti, T. Rubehn, H. Sann, A. Schuttauf, W. Seidel, W. Trautmann, and A. Worner, Nucl. Phys. **A584**, 737 (1995).
[29] V. Weisskopf, Phys. Rev. **52**, 295 (1937).
[30] H. A. Bethe, Phys. Rev. **50**, 332 (1936).
[31] N. Bohr and J. A. Wheeler, Phys. Rev. **56**, 426 (1939).
[32] J. Benlliure, P. Armbruster, M. Bernas, A. Boudard, T. Enqvist, R. Legrain, S. Leray, F. Rejmund, K. H. Schmidt, C. Stéphan, L. Tassan-Got, and C. Volant, Nucl. Phys. **A700**, 469 (2002).
[33] H. A. Kramers, Physica (Amsterdam) **4**, 284 (1940).
[34] P. Grangé, J. Q. Li, and H. A. Weidenmüller, Phys. Rev. C **27**, 2063 (1983).
[35] EOS Collaboration, R. P. Scharenberg *et al.*, Phys. Rev. C **64**, 054602 (2001).
[36] C. A. Bertulani and G. Baur, Phys. Rep. **163**, 299 (1988).
[37] G. Baur, K. Hencken, and D. Trautmann, J. Phys. G **24**, 1657 (1998).
[38] F. Krauss, M. Greiner, and G. Soff, Prog. Part. Nucl. Phys. **39**, 503 (1997).
[39] I. A. Pshenichnov, I. N. Mishustin, J. P. Bondorf, A. S. Botvina, and A. S. Iljinov, Phys. Rev. C **60**, 044901 (1999).
[40] I. A. Pshenichnov, I. N. Mishustin, J. P. Bondorf, A. S. Botvina, and A. S. Iljinov, Phys. Rev. C **57**, 1920 (1998).
[41] W. J. Llope and P. Braun-Munzinger, Phys. Rev. C **41**, 2644 (1990).
[42] A. S. Iljinov, I. A. Pshenichnov, N. Bianchi, E. De Sanctis, V. Muccifora, M. Mirazita, and P. Rossi, Nucl. Phys. **A616**, 575 (1997).
[43] P. B. Price, R. Guoxiao, and W. T. Williams, Phys. Rev. Lett. **61**, 2193 (1988).
[44] K. Sakamoto, S. R. Sarkar, Y. Oura, H. Haba, H. Matsumura, Y. Miyamoto, S. Shibata, M. Furukawa, and I. Fujiwara, Phys. Rev. C **59**, 1497 (1999).
[45] S. Datz, J. R. Beene, H. F. Krause, C. R. Vane, P. Grafström, H. Knudsen, and R. H. Schuch, Phys. Rev. Lett. **79**, 3355 (1997).
[46] L. Y. Geer, J. Klarmann, B. S. Nilsen, C. J. Waddington, W. R. Binns, J. R. Cummings, and T. L. Garrard, Phys. Rev. C **52**, 334 (1995).
[47] K. Sümmerer, J. Reinhold, M. Fauerbach, J. Friese, H. Geissel, H. J. Körner, G. Münzenberg, R. Schneider, and K. Zeitelhack, Phys. Rev. C **52**, 1106 (1995).
[48] J. R. Cummings, W. R. Binns, T. L. Garrard, M. H. Israel, J. Klarmann, E. C. Stone, and C. J. Waddington, Phys. Rev. C **42**, 2508 (1990).
[49] C. J. Waddington, J. R. Cummings, B. S. Nilsen, and T. L. Garrard, Phys. Rev. C **61**, 024910 (2000).
[50] S. E. Hirzebruch, E. Becker, G. Hüntrup, T. Streibel, E. Winkel, and W. Heinrich, Phys. Rev. C **51**, 2085 (1995).
[51] C. A. Bertulani and D. S. Dolci, Nucl. Phys. **A674**, 527 (2000).
[52] K.-H. Schmidt, M. V. Ricciardi, A. S. Botvina, and T. Enqvist, Nucl. Phys. **A710**, 157 (2002).